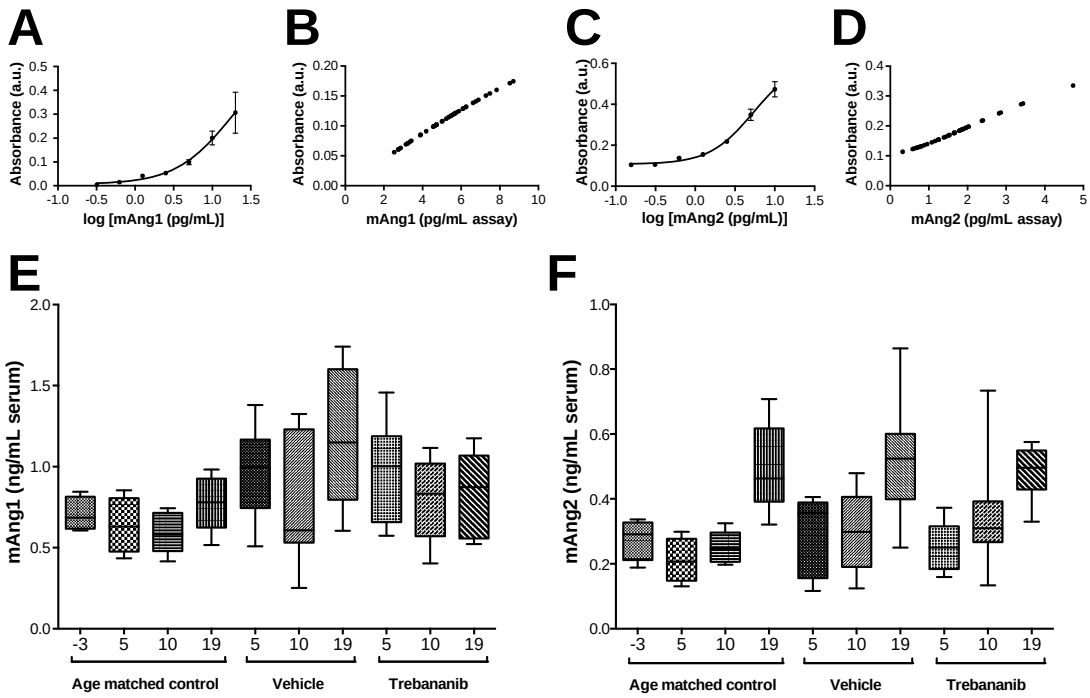

Supplemental Fig. 1. Standard curves and raw data from determination of mAng1 and mAng2 in serum by ELISA. (A) Standard curve for mAng1 (pg / mL in assay). (B) Raw data for mAng1. (C) Standard curve for mAng2 (pg / mL in assay) (D) Raw data for mAng2. Values of "pg / mL assay" were converted to "ng / mL serum" stated in the main manuscript by accounting for the dilution factor of 1:200. (E) Serum mAng1 (ng / mL) across all treatment groups. The levels of mAng1 at day 5 of tumor development were 0.69 ± 0.12, 0.95 ± 0.09 and 0.98 ± 0.10 ng / mL serum in healthy, vehicle and Trebananib treated groups respectively (F) Serum mAng2 (ng / mL) across all treatment groups. The levels of serum mAng2 at day 5 of tumor development were 0.21 ± 0.05, 0.29 ± 0.04 and 0.25 ± 0.02 ng / mL serum in healthy, vehicle and Trebananib treated mice respectively. Numbers on abscissa refer to days post

implantation. Statistical significance of ELISA data is discussed in the main text.

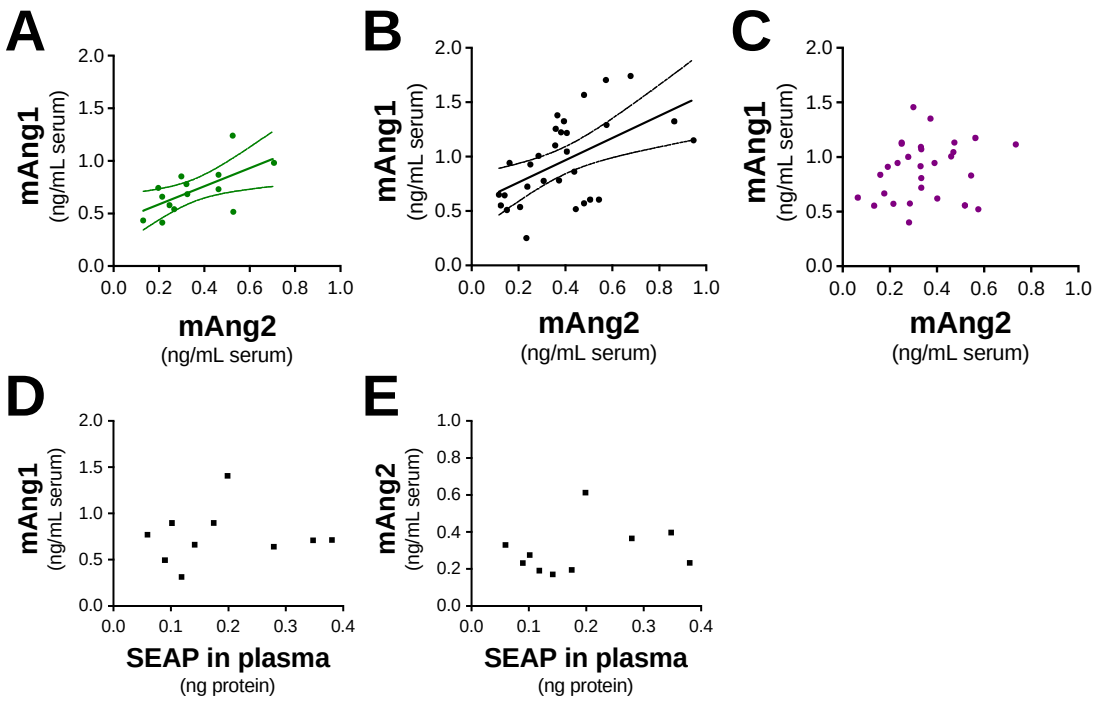

Supplemental Fig. 2. Correlations between circulating levels of mAng1, mAng2 and SEAP. (A, B) In the healthy control and vehicle-treated groups, the circulating levels of mAng1 and mAng2 are moderately correlated (Healthy: n = 14, $r_s = 0.6238$, p = 0.0171; Vehicle: n = 30, $r_s = 0.5122$, p = 0.0038), but this was not the case in the Trebananib group (C) (n = 30, $r_s = 0.1468$, p = 0.4388). Plasma SEAP levels do not correlate with the decrease in mAng1 protein detectable in serum (D), or the increase in mAng2 protein (E). "SEAP in plasma" quoted as ng protein detected in 5 µL of isolated plasma.

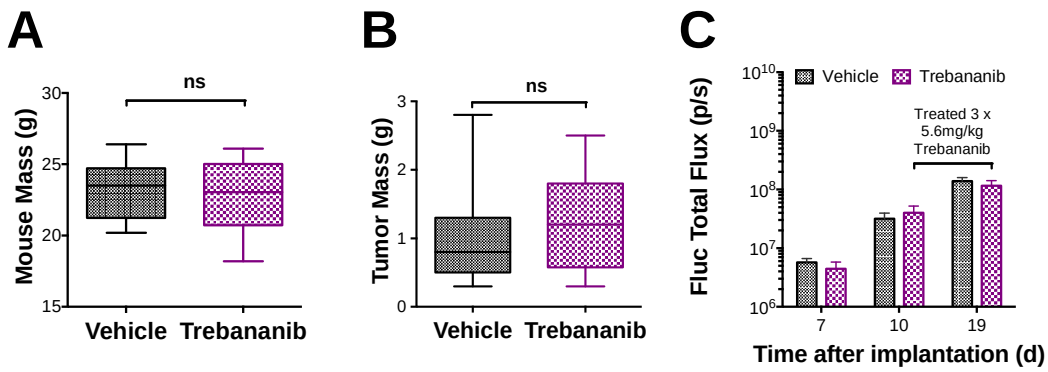

Supplemental Fig. 3. Treatment with Trebananib does not cause weight loss in the mice (A) or impact the final tumor mass (B) / burden at day 19 (C).

Tumor burden was assessed using bioluminescence imaging (BLI) and used to randomize mice at day 10. Treatment did not induce a statistically significant difference between the groups by day 19. Due to the fast growing nature of this tumor model, it was not possible to monitor the mice beyond day 21. In a small subset of mice maintained to day 21 (n = 3), the average tumor mass was 1.5 g in vehicle treated mice and 0.8 g in Trebananib treated mice, indicating a trend towards growth retardation.

Supplemental Table 1: Human proteins Ang1, Ang2, CA125 and VEGF were not detectable in serum but some were found in cell culture media. 10^5 A2780-SEAP-FLuc-EGFP cells were seeded in each well of a 12 well plate. 10 μL of Trebananib stock solution at 1.1 mg/mL was added to Trebananib treated wells at 6 h after seeding. Empty wells containing complete media were also assayed. These data indicate that A2780-SEAP-FLuc-EGFP cells do not secrete human Ang1, Ang2 or CA125; the only detectable angiopoietin was present in the complete media itself. Human VEGF was detectable in cell culture media, but not in media alone, indicating that the cells do secrete a low level of human VEGF. Values are in pg / mL media, n.d. = not detectable.

Protein	24 h			72 h		
	Vehicle	Trebananib	Media Alone	Vehicle	Trebananib	Media Alone
Ang1	963	641	922	1310	1002	932
Ang2	212	269	617	90	148	621
CA125	n.d.					
VEGF	1261	1176	n.d.	6980	6638	n.d.

Supplemental Video 1: Photoacoustic tomography volume illustrating region of interest positioning (horizontal axis). This movie illustrates the positioning of the regions of interest drawn over the tumor bearing ovary and the contralateral side in order to quantify the photoacoustic imaging data. The region on the contralateral side is used for normalization of the imaging signal, to account for differences in the overall image intensity between different imaging sessions and/or mice that can be observed in some data sets.

Note that all movies are generated using OsiriX movie export function from the 3D maximum intensity projection tool.

Animal model preparation

The human ovarian carcinoma A2780 cell line (genetically authenticated by IDEXX Laboratories Ltd., October 2014) was stably transfected with an optical imaging reporter, enhanced green fluorescent protein (eGFP) fused to firefly luciferase (FLuc) fusion protein, and secreted alkaline phosphatase (SEAP) to generate the A2780-SEAP-FLuc-eGFP cell line (*1*) used in these studies. These constructs respectively enable: FAC sorting and visualization of culture cells (eGFP), noninvasive visualization and quantification of viable tumor burden in cell culture and in vivo (Fluc) and monitoring of tumor burden via blood sampling (SEAP) (*2*). We used a dual constitutive ubiquitin promoter approach to obtain high expressing levels of both SEAP and the bifusion Fluc-eGFP similar to dual promoter approaches previously used in the literature with the CMV promoter (*3*) and bi-tri fusion reporter gene strategies we have previously described (*4*). No mycoplasma contamination was determined. All cell culture materials were purchased from Invitrogen Life Technologies. Cells were cultured in RPMI 1640 media supplemented with 10% fetal bovine serum and a 1% penicillin and streptomycin solution, under sterile conditions and maintained in a 5% CO_2-humidified incubator at 37°C. For implantation, cells at 80% confluence were trypsinized and 5 x 10^5 cells were resuspended in 10 μL phosphate buffered saline (PBS).

To enable access to the ovary for implantation, mice were anesthetized using 2 % isoflurane mixed with oxygen and the surgical site was sterilized with swabs saturated with betadine (Purdue Products) then alcohol (BD). Using sterile instruments, a small vertical incision was made in the dorsomedial position, immediately above the ovarian fat pad (*1,5,6*). After making a small incision in the underlying abdominal muscle lining, sterile forceps were used to retract the ovarian

fat pad through the incision and expose the ovary. A cell suspension of 5 x 10^5 cells was delivered using a dissection microscope to guide the gentle insertion of a 31 G needle (BD) directly into the bursa. The incision in the muscle was closed with sutures (CP-B421A-04; CP Medical) and the skin with surgical wound autoclips (427631; BD Medical). Mice were monitored for 2 hours following surgery and then daily for signs of morbidity.

Blood sampling and biomarker assays

To study the effects of Trebananib on biomarker levels, blood sampling was performed under the anesthesia regimen described above. Blood was obtained using a 5 mm lancet (Goldenrod; Medipoint, Inc.) via the submandibular facial vein, up to a maximum of 7.5% circulating blood volume per week. For plasma analysis of SEAP concentration, blood was collected in a plasma separation tube containing lithium heparin (02-675-182; BD Medical) according to the manufacturer protocol. For serum analysis, the collection tube contained a serum-gel clotting activator (41.1378.005; Sarstedt) and was allowed to stand at room temperature for at least 1 hour before centrifugation at 12,000 rpm for 10 minutes. Serum samples were obtained at day 5, 10 and 19 only, due to the larger volumes required, in accordance with animal welfare guidelines. In both cases the supernatant was collected immediately and stored at -80°C for later use.

Plasma samples were assayed for the presence of Serum Alkaline Phosphatase (SEAP) using the Great EscAPe SEAP Chemiluminescence Assay 2.0 (Clontech). Serum samples were assayed for human (A2780 cell line derived) factors using Quantikine ELISA kits (R&D Systems) for human CA125, VEGF, Ang1 and Ang2 according to manufacturer protocols. No human factors were detected in serum, although some could be detected in cell culture (Supplemental Table 1). The lack of

CA125 expression by A2780 cells confirms previous findings (*7*). Serum samples were also assayed for murine (host endothelial cell derived factors) Ang1 and Ang2 using ELISA kits (Cusa Bio, obtained via Cosmo Bio USA) according to manufacturer protocols. All biological replicates were then assayed in duplicate.

Photoacoustic tomography

The Nexus 128 delivers laser light, provided by a tunable (680 – 950 nm), pulsed Nd:YAG laser (OPOTEK Inc.), from below the sample via a planoconvex lens at the bottom of the hemisphere, providing a light beam of approximately 20 mm in diameter at the animal bed. The detection system consists of an array of 128 individual, unfocused transducers (center frequency = 5 MHz) positioned in a spiral pattern on a hemispherical bowl with a 101 mm radius of curvature. The transducers are ultrasound coupled to the mouse laying within the animal bed by filling the bowl with water, which is maintained at 38°C by a pumping system. A small amount of water (3 – 5 mL) is added to the animal bed to provide the final coupling between the bed and the mouse. The final temperature of the mice was in the range 36-37°C. The laser energy delivered by the system is monitored via a beam splitter in the light path throughout the experiment and an average value recorded for each angular view. The supplied energy is normalized on a per view basis during image reconstruction.

The tumor (T) is outlined using a 3D region of interest; it is located immediately below the superficial vessels (SV) and often encompasses part of the ovarian vessels (OV) as shown in Fig. 2. The voxel size for all images is 100 x 100 x 100 μm^3 and the full width of the reconstruction volume is 2.56 cm. Regions of interest were drawn over equivalent regions about both the tumor and contralateral ovary. In the x (medial-lateral), y (superior-inferior) and z (anterior-posterior) directions, the region was bounded by: the inferior vena cava (medial) and skin layer

of the mouse (lateral); the kidneys (superior) and the line defined by the lower end of the spleen (inferior); the superficial skin vessels (anterior) and the ovarian vessels (posterior). Where relevant, data was normalized to an equal sized region placed on the contralateral side of the mouse.

Histologic Tumor Analysis

Hematoxylin and eosin stained sections were scanned (Hamamatsu Nanozoomer; NDP View) and quantified by percent necrotic area in whole tumor sections (NIH ImageJ, Fiji). Imaging of immunofluorescence stained sections was performed on a Zeiss LSM510 Meta inverted confocal microscope and 16-bit images were recorded. A minimum of three regions of 883 x 883 μm^2 (2 x 2 tiled image) were analyzed per section, with one taken at the center and two at the periphery of the tumor, and at least four sections (cut at approximately equal intervals) were stained per tumor. Images were analyzed in NIH ImageJ (Fiji) by converting to 8-bit, creating a mask (threshold 8 – 255) then using analyze particles (size = 10 – infinity) to determine count, total area and average size. Vessel density was expressed as the CD31 positive count per square micron analyzed (no. vessels / μm^2). The overlap of CD31 and desmin staining was quantified by performing a boolean AND of the two mask images then repeating the analyze particles procedure (size = 0 – infinity) to determine total overlapping area, then dividing by the total CD31 positive vessel area to assess percentage overlap.

For CD31 immunofluorescence staining, tumor sections from paraffin embedded tissues were deparaffinized with Safeclear (23-314-629; Fisher Healthcare) then rehydrated with alcohols; antigen retrieval was performed in Tris-HCl buffer at pH 9 using a decloaking chamber (NxGen; Biocare Medical). Frozen sections, used for combined CD31 and desmin immunofluorescence staining, did not undergo this

procedure. Slides were incubated with permeabilization buffer (0.5 % Triton X-100 in 1x PBS) for 10 minutes then blocking buffer (3 % bovine serum albumin, 3% donkey serum, 3% goat serum in 1x PBS) for 30 minutes before overnight incubation at 4 °C with the primary antibody (rabbit polyclonal to CD31, 1:100 dilution; ab28364, Abcam). The secondary antibody (goat anti-rat IgG Alexa Fluor 546, 1:250 dilution; A11081, Invitrogen Life Technologies) was applied for 30 minutes at room temperature. Slides were washed with 1x PBS between each step. Sections were mounted in Slowfade Gold reagent (S36936; Invitrogen Life Technologies) with 22x60-1.5 Fisherbrand microscope cover glass.

For co-localization of CD31 and desmin staining, frozen tissues were sectioned at 10 μm thickness using a Microm 550M Cryostat microtome. The sections were stained as above, using primary rat anti-mouse CD31 (1:250 dilution; 557355, BD Pharmingen) and rabbit anti-mouse desmin (1:100 dilution; ab15200, Abcam) then secondary donkey anti-rat IgG Alexa Fluor 488 (1:250 dilution; A21208, Invitrogen Life Technologies) and goat anti-rabbit IgG Alexa Fluor 546 (1:250 dilution; A11010, Invitrogen Life Technologies). Alexa Fluor 633 Phalloidin (A22284, Invitrogen Life Technologies), a high affinity F-actin probe, was used as a tissue counterstain.

References

1. Hori SS, Lutz AM, Paulmurugan R, et al. A mouse model integrated with a mathematical model for studying early cancer detection. 2015. In preparation.

2. Nilsson EE, Westfall SD, McDonald C, et al. An in vivo mouse reporter gene (human secreted alkaline phosphatase) model to monitor ovarian tumor growth and response to therapeutics. *Cancer Chemoth Pharm.* 2002;49:93-100.

3. Zinn KR, Chaudhuri TR, Krasnykh VN, et al. Gamma camera dual imaging with a somatostatin receptor and thymidine kinase after gene transfer with a bicistronic adenovirus in mice. *Radiology*. 2002;223:417-425.

4. Ray P, De A, Min JJ, et al. Imaging tri-fusion multimodality reporter gene expression in living subjects. *Cancer Res.* 2004;64:1323-1330.

5. Connolly DC, Hensley HH. Xenograft and Transgenic Mouse Models of Epithelial Ovarian Cancer and Non Invasive Imaging Modalities to Monitor Ovarian Tumor Growth In situ -Applications in Evaluating Novel Therapeutic Agents. *Current Protocols in Pharmacology.* 2009;45:14 12 11-14 12 26.

6. Nunez-Cruz S, Connolly DC, Scholler N. An Orthotopic Model of Serous Ovarian Cancer in Immunocompetent Mice for in vivo Tumor Imaging and Monitoring of Tumor Immune Responses. *J Vis Exp.* 2010;45:e2146.

7. Shaw TJ, Senterman MK, Dawson K, et al. Characterization of intraperitoneal, orthotopic, and metastatic xenograft models of human ovarian cancer. *Mol Ther*. 2004;10:1032-1042.